

Electronic structure and magnetic ordering of NiN and Ni₂N from first principles

Abdesalem Houari,^{1,*} Samir F. Matar,^{2,†} and Volker Eyert^{3,‡}

¹*Theoretical Physics Laboratory, Department of Physics, University of Bejaia, Bejaia, Algeria*

²*Lebanese German University, LGU, Sahel-Alma Campus, Jounieh, Lebanon*

³*Materials Design SARL, 92120 Montrouge, France*

(Dated: November 27, 2018)

The results of first-principles electronic structure calculations for the nitrogen-rich nickel nitrides NiN and Ni₂N are presented. The calculations are based on density functional theory and used the generalized gradient approximation (GGA) as well as the GGA+*U* approach. The latter turned out to be crucial for a correct description of the crystal phase stability and magnetic instabilities of both compounds. While for NiN GGA calculations predict a non-magnetic ground state with the zincblende structure, GGA+*U* calculations result in a half-metallic ferromagnet with the rocksalt structure in line with indications from the neighboring transition-metal nitrides making NiN a possible candidate for spin-filter devices. For Ni₂N GGA calculations likewise lead to a non-magnetic behavior, which is contrasted with a ferrimagnetic ordering obtained from the GGA+*U* approach. This ground state results from complex three-dimensional exchange interaction via σ -type and π -type overlap of the Ni 3*d* orbitals with the N 2*p* orbitals and may explain the reported sensitivity of the magnetic ordering to details of the crystal structure. For both nitrides, experimental data are called for to confirm our predictions.

PACS numbers: 71.10.-w, 71.15.Mb, 71.15.Nc

Keywords: NiN, Ni₂N, Ni₃N, transition-metal nitrides, magnetism, electronic structure calculations

I. INTRODUCTION

As compared to the huge class of transition-metal oxides the respective nitrides have been much less studied due in part to comparably greater difficulties to synthesize these systems as a consequence of the high stability of the N₂ molecule. Nevertheless, a wide spectrum of promising electronic, magnetic, and mechanical properties generated high interest in the nitrides since long.¹ This applies especially to the 3*d* transition metal nitrides, some of which show superconducting phases and magnetic instabilities while others allow application, e.g. as hard materials, anticorrosion coatings, electrical contacts, diffusion barriers, catalysts, sensors, and fuel cells.^{2,3} Yet, in particular the late transition-metal nitrides long resisted successful synthesis, a fact attributed to the increased filling of their antibonding 3*d*-2*p* states.⁴ For this reason, the thermodynamic stability, crystal structures as well as the electronic and magnetic properties of these latter binaries have been a matter of dispute for long and only recently work on these compounds has started to measure up with the increasing interest. This holds true also for the nickel nitrides. Published phase diagrams include mainly three different nitride phases, namely, Ni₈N, Ni₄N, and Ni₃N.^{5,6} However, even the thermodynamic stabilities of some of these phases were controversially discussed for a long time.

Probably the best studied nickel nitride is Ni₃N, which was obtained already quite early from nickel metal and ammonia.⁷ From x-ray diffraction, the Ni sublattice was identified as a hexagonal close-packed structure with lattice parameters $a = 2.664 \text{ \AA}$ and $c = 4.298 \text{ \AA}$.⁷ The nitrogen atoms intercalate into the metal sublattice and occupy the octahedral interstices. As a result, the crystal

structure of Ni₃N assumes the hexagonal ϵ -Fe₃N structure with space group P6₃22 and the basal-plane lattice parameter increased by a factor $\sqrt{3}$, i.e. to $a \approx 4.62 \text{ \AA}$.⁷⁻⁹ Ni₃N like many other binary 3*d* transition-metal nitrides thus falls into the broad class of metallic interstitial compounds with a metal sublattice, which is characteristic of a simple metal (e.g. fcc, bcc, or hcp), and nitrogen atoms located at the interstices.⁹ Possible disorder of the nitrogen atoms was addressed in detail by Leineweber *et al.*, who investigated the ϵ -phase nitrides of Mn, Fe, and Ni using neutron powder diffraction. They found an order-disorder transition at 550 K in Mn₃N_{1.17}, partial disorder with increasing temperature in Fe₃N_{1+x}, and complete order in Ni₃N.⁸⁻¹⁰ The overall trend of this behavior was explained by the decrease of lattice parameters along the series, which causes decrease in N-N distances. The resulting increase in repulsive interactions between the interstitial atoms would then cause their ordering.⁸ The hexagonal ϵ -Fe₃N structure of Ni₃N and the above given lattice parameters were subsequently confirmed by several groups using powder and nanocrystalline samples as well as thin films obtained from various synthesization processes and characterized by x-ray, neutron, and electron diffraction.^{3,6,9-18} Nevertheless, Ni₃N was also reported to thermally decompose at temperatures above 600-680 K.^{7-9,19} Juza and Sachsze also mentioned the metallic bonding in this nickel nitride, which contrasts the ionic metal-nitrogen bonding reported for Cu₃N.⁷

Only few studies focused on the magnetic properties of Ni₃N. While Gajbhiye *et al.* found stable ferromagnetic order below $T_C = 634 \text{ K}$, Vempaire *et al.* as well as Leineweber *et al.* did not observe any indications for a magnetic instability.^{3,10,12,14,15,17} This finding was also supported by first principles calculations, which at-

tributed the suppression of magnetic order to delocalization of the electronic states due to the strong Ni $3d$ -N $2p$ hybridization.^{12,14,15,20,21}

In contrast to Ni₃N, Ni₄N and Ni₈N were much less studied since they appeared mainly as intermediate phases during the decomposition of the former compound.^{3,19,22,23} Nevertheless, Ni₄N was characterized as having a cubic lattice with lattice constant $a = 3.77 \text{ \AA}$.⁶ From first principles calculations, both Ni₄N and Ni₈N were predicted to have non-zero magnetization,^{20,21,24–26} similar to the neighboring transition-metal nitrides M₄N (M = Mn, Fe, Co), which have been studied by various authors.^{26–30}

The nickel nitrides with a higher nitrogen concentration were even less studied than the Ni-rich nitrides. Ni₂N assumes a simple tetragonal structure with lattice parameters $a = 2.80 \text{ \AA}$ and $c = 3.66 \text{ \AA}$ and space group P4/mmm.¹¹ The magnetic properties of Ni₂N are still unclear. While measurements on thin layers as well as first principles calculations using the generalized-gradient approximation (GGA) of density functional theory (DFT) did not show any magnetic order, more recent experiments indicated spin-glass like behavior and proximity of a magnetic instability at increased volume.^{14,15,31}

Finally, like CuN nickel mononitride seems not to have been investigated experimentally so far.³² However, first principles calculations using the local density approximation (LDA) or the GGA showed that NiN assumes a metallic, non-magnetic ground state within the zincblende structure like the neighboring mononitrides CoN and CuN.^{32,33} In contrast, CrN showed antiferromagnetic ordering in an orthorhombic structure.³⁴

The present work, which is part of a broader set of investigations on magnetic transition-metal nitrides,^{29,35–39} focuses on the thermodynamic stability as well as the electronic and magnetic properties of NiN and Ni₂N. To this end we apply electronic structure calculations as based on density functional theory within the generalized-gradient approximation (GGA). However, in the course of our work it became obvious that a successful description of both compounds requires to go beyond and to apply the GGA+ U approach in order to take proper account of the local electronic correlations impacting the electronic and magnetic properties. In order to be consistent and underline the validity of our approach, we complement the calculations for the above N-rich compounds by computations for Ni₃N.

The paper is organized as follows: After describing the theoretical methods and computational details in Sec. II, we present the calculated results obtained for all three compounds in Sec. III before concluding in Sec. IV.

II. COMPUTATIONAL METHODS

The first principles calculations were based on density functional theory^{40,41} with exchange-correlation effects accounted for by the PBE parametrization of the gen-

eralized gradient approximation (GGA) as proposed by Perdew, Burke, and Ernzerhof.⁴² Motivated by a large amount of studies on the paradigmatic antiferromagnetic insulator NiO, for which taking account of local electronic correlations via a GGA+ U treatment turned out to be crucial, we complemented the GGA calculations by calculations using the GGA+ U method.^{43,44} Following previous GGA+ U investigations on NiO we selected $U = 6.0 \text{ eV}$ and $J = 0.95 \text{ eV}$ for the Ni $3d$ orbitals.^{45–48} However, to check the sensitivity of the results to the choice of these parameters, we also performed some calculations with $U = 4.0 \text{ eV}$ and $J = 0.64 \text{ eV}$. For each set of U and J we first performed a structure relaxation, which was then followed by a calculation of the electronic and magnetic properties. In doing so we even distinguished spin-degenerate and spin-polarized situations, i.e. both structure relaxation and calculation of the electronic and magnetic properties were performed separately for these two cases. As a consequence, there is an intimate connection between U and J , the crystal structure parameters, and the electronic structure. For the double counting correction the fully localized limit was used.^{44,49–51}

Two complementary first principles methods were employed: In a first step, the Vienna Ab initio Simulation Program (VASP) as implemented in the MedeA[®] computational environment of Materials Design was used to perform total-energy and force calculations aiming at a relaxation of the structures.^{52,53} The single-particle equations were solved using the projector-augmented wave (PAW) method with a plane-wave basis and a cutoff of 520 eV.^{54,55} All calculations were converged until the total-energy difference between two consecutive iterations was lower than 10^{-5} eV and the forces on the atoms were converged to 0.02 eV/\AA . The Brillouin zone of NiN was sampled using a Monkhorst-Pack mesh with a spacing below 0.2 \AA^{-1} leading to $15 \times 15 \times 15$ \mathbf{k} -points for the rocksalt structure, $13 \times 13 \times 13$ \mathbf{k} -points for the zincblende and cesium chloride structures, and $13 \times 13 \times 7$ \mathbf{k} -points for the wurtzite structure.⁵⁶ For Ni₂N and Ni₃N this spacing led to $13 \times 13 \times 9$ and $9 \times 9 \times 9$ \mathbf{k} -points, respectively.

Once the equilibrium structures were known, analysis of the electronic structure, magnetic ordering, and chemical bonding was carried out using the full-potential augmented spherical wave (ASW) method in its scalar-relativistic implementation.^{57,58} In the ASW method, the wave function is expanded in atom-centered augmented spherical waves, which are Hankel functions and numerical solutions of Schrödinger's equation, respectively, outside and inside the so-called augmentation spheres. In order to optimize the basis set and enhance the variational freedom, additional augmented spherical waves were placed at carefully selected interstitial sites. The choice of these sites as well as the augmentation radii were automatically determined using the sphere-geometry optimization algorithm.⁵⁹ Self-consistency was achieved by a highly efficient algorithm for convergence acceleration⁶⁰ until the variation of the atomic charges

was smaller than 10^{-8} electrons and the variation of the total energy was smaller than 10^{-8} Ryd. Brillouin zone integrations were performed using the linear tetrahedron method⁶¹ with up to $26 \times 26 \times 26$ \mathbf{k} -points for the rocksalt structure, $24 \times 24 \times 24$ \mathbf{k} -points for the zincblende and cesium chloride structures, and $23 \times 23 \times 12$ \mathbf{k} -points for the wurtzite structure of NiN. In contrast, for Ni₂N and Ni₃N up to $22 \times 22 \times 17$ and $16 \times 16 \times 15$ \mathbf{k} -points, respectively, were used. Increasing the number of \mathbf{k} -points in several steps up to the just mentioned maximum settings allowed to control convergence of the results with respect to the density of the Brillouin-zone mesh.

III. RESULTS AND DISCUSSIONS

A. Ni₃N

In order to obtain a first impression of the thermodynamic stability and electronic structure of the nickel nitrides and to lay ground for the subsequent discussion of the nitrogen-rich class members we start out considering Ni₃N. From structure relaxations using VASP together with both GGA and GGA+ U lattice parameters of $a = 4.617$ Å, $c = 4.306$ Å and $a = 4.512$ Å, $c = 4.193$ Å, respectively, were obtained. As expected, the GGA+ U results are slightly smaller than the GGA values due to the stronger localization of the Ni 3d orbitals. The internal parameter fixing the position of the Ni atoms was calculated as $x_M = 0.330$ and $x_M = 0.333$ using the GGA and GGA+ U method, respectively. Both sets are close to the experimental data of $a = 4.622$ Å, $c = 4.306$ Å, and $x_M = 0.3279$.⁹ The enthalpy of formation as compared to the elements in their standard state (ferromagnetic face-centered cubic Ni and N₂ molecule) was calculated to +0.10 eV and -0.08 eV per formula unit from GGA and GGA+ U , respectively. Hence, while both values are close to each other, the negative value obtained from the GGA+ U method confirms the necessity to go beyond the GGA. Finally, we point out that neither of these approaches led to magnetic order, in agreement with the experimental findings.

The electronic densities of states as obtained from spin-degenerate ASW calculations using the GGA+ U approach, which turned out to be very similar to those resulting from the GGA calculations, are displayed in Fig. 1. We distinguish the in-plane Ni 3d_{xy, x²-y²}, out-of-plane Ni 3d_{3z²-r²}, and the mixed Ni 3d_{xz, yz} orbitals. Since the out-of-plane orbitals mediate weak overlap perpendicular to the basal plane of the hexagonal unit cell with like orbitals of Ni sites neighboring along the c axis, their partial densities of states are essentially confined to the central energy interval from -5 eV to the Fermi energy, where N 2p contributions are small. In contrast, the in-plane and mixed orbitals, in addition to dominating in the central energy interval, also contribute to the energy intervals from about -9.5 eV to -6.5 eV and from the Fermi energy to about +2 eV, where they complement

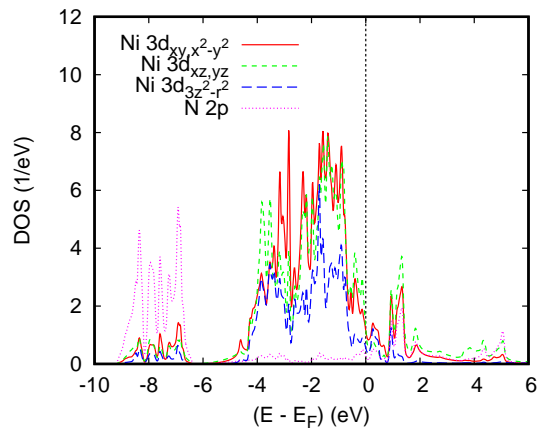


FIG. 1: Partial densities of states of Ni₃N as arising from the GGA+ U calculations. In all figures a Gaussian broadening of 50 meV was used.

the strong N 2p partial densities of states. This complementarity results from the strong spatial overlap of these orbitals, which leads to bonding and antibonding manifolds in the lower and upper part of the spectrum.

B. Ni₂N

According to recent measurements, Ni₂N assumes a simple tetragonal structure with space group P4/mmm and lattice parameters $a = 2.815$ Å and $c = 3.665$ Å.^{31,62} The structure is displayed in Fig. 2. The Ni atoms oc-

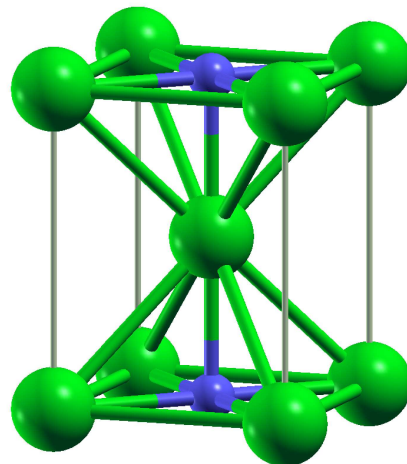


FIG. 2: Crystal structure of Ni₂N. Nickel and nitrogen atoms are given in green and blue, respectively.

cupy the Wyckoff positions (1a) and (1d) and thus are located at the corner (labeled Ni1 below) and the center (Ni2), respectively, of the unit cell, whereas the nitrogen atoms occupy the Wyckoff position (1c) at the center of the basal plane. Hence, the two Ni atoms are not

equivalent by symmetry but would be and form a body-centered tetragonal lattice were it not for the nitrogen atoms. As well known, in the tetragonal crystal system the body-centered lattice is identical to a face-centered lattice with the conventional-cell vectors rotated by 45° about the tetragonal c axis, the lattice parameter a increased by a factor of $\sqrt{2}$, and the c/a ratio reduced by the same factor.⁶³ In the present case, this would give rise to a face-centered tetragonal lattice with one nickel atom per primitive cell and lattice parameters $a = 3.981 \text{ \AA}$ and $c = 3.665 \text{ \AA}$, i.e. $c/a = 0.921$. These numbers have to be contrasted with the lattice parameter $a = 3.524 \text{ \AA}$ found for face-centered cubic Ni. Starting from that lattice, the nitrogen atoms are inserted into part of the octahedral voids, specifically at the centers of eight out of twelve edges of the cubic cell and, hence, give rise to a planar arrangement. As a consequence, strong elongation by about 13% of the corresponding in-plane lattice parameters of the original face-centered cubic lattice of elemental Ni is found, whereas elongation along the third axis amounts to only 4%. Obviously, even without the insertion of nitrogen such geometric changes would have a strong impact on the ferromagnetic ordering. In particular, the lattice expansion would cause narrowing of the electronic bands, hence, overall increase of the density of states, and via the Stoner criterion strengthening of the ferromagnetic order. Indeed, as calculations for elemental nickel within the face-centered cubic and tetragonal lattices reveal, the lattice expansion leads to increase of the ferromagnetic moment from $0.63\mu_B$ to $0.82\mu_B$ per atom.

As was also mentioned above, measurements on thin films gave no hint at long-range magnetic order.^{14,15,64} While this finding was supported by first principles calculations as based on the GGA,^{14,15,31} magnetization measurements on bulk samples revealed spin-glass like behavior and initiated calculations, which showed onset of ferromagnetic order for an isotropically expanded lattice.³¹

Again, in a first step we performed structure relaxations using VASP together with both GGA and GGA+ U . From the former, lattice parameters of $a = 2.815 \text{ \AA}$ and $c = 3.644 \text{ \AA}$ were obtained. In contrast, the latter led to $a = 2.817 \text{ \AA}$ and $c = 3.589 \text{ \AA}$, which as expected are smaller than the GGA values due to the stronger localization of the Ni $3d$ orbitals. Both results are in very good agreement with the measured values. The enthalpy of formation as compared to the elements in their standard state was calculated as $+0.46 \text{ eV}$ and $+0.03 \text{ eV}$ per formula unit from GGA and GGA+ U , respectively. Again, the difference between these values underlines the necessity to use the GGA+ U approach, while the fact that the latter value is still slightly positive reflects the conflicting reports about the ground state of this material. Finally, we point out that while from the GGA calculations no magnetic order could be obtained, the GGA+ U calculations gave rise to a ferrimagnetic ground state. Our results are thus in line with the indications of a magnetic instability found by Nishi-

hara and coworkers.³¹ The ferrimagnetic ordering found from the GGA+ U calculations also explains the larger difference between the GGA and GGA+ U values of the enthalpy of formation as compared to the corresponding results for Ni_3N .

The electronic densities of states as obtained from spin-polarized ASW calculations using the GGA+ U approach are displayed in Figs. 3, 4, and 5. In Fig. 3, we distin-

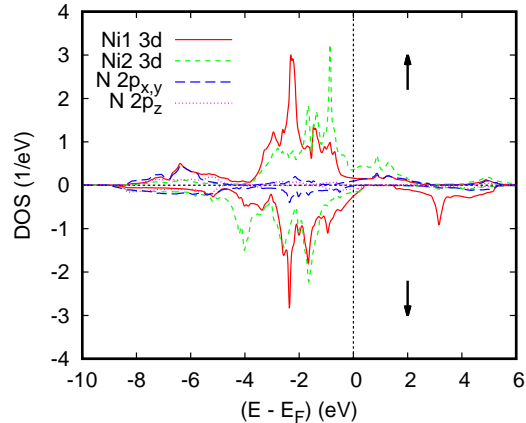


FIG. 3: Partial densities of states of Ni_2N as arising from the GGA+ U calculations.

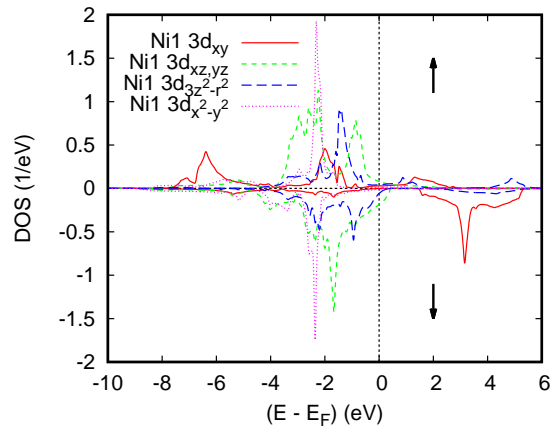


FIG. 4: Partial Ni1 densities of states of Ni_2N as arising from the GGA+ U calculations.

guish the partial densities of states due to the N $2p_{x,y}$ and $2p_z$ orbitals, which form σ -type bonds with the Ni1 $3d_{xy}$ and Ni2 $3d_{3z^2-r^2}$ orbitals, respectively. In case of Ni1 this overlap gives rise to distinct spin-up bonding and spin-down antibonding peaks at about -6.5 and $+3 \text{ eV}$, respectively, which are also clearly observed in Fig. 4. In addition, it causes antiparallel alignment of the local magnetic moments of $+0.50\mu_B$ and $-0.26\mu_B$, which are carried exclusively by the Ni1 $3d_{xy}$ and the N $2p_{x,y}$ orbitals, respectively. In contrast, the local magnetic moments of $-0.97\mu_B$ at the Ni2 sites are due to the

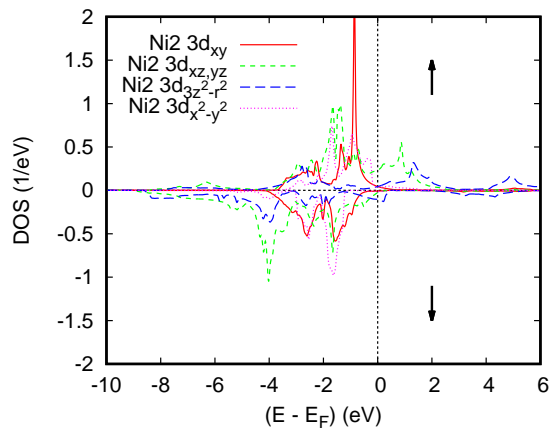


FIG. 5: Partial Ni2 densities of states of Ni₂N as arising from the GGA+*U* calculations.

$3d_{3z^2-r^2}$, $3d_{xz}$, and $3d_{yz}$ states but do not polarize the N $2p_z$ states. Thus, a rather complex magnetic behavior is observed, where the magnetic moments at the Ni1 sites interact only within the tetragonal basal plane via σ -type overlap with the in-plane N $p_{x,y}$ orbitals. In contrast, the magnetic moments at the Ni2 sites are subject to two different kinds of exchange interactions, namely, via σ -type overlap of the Ni2 $3d_{3z^2-r^2}$ with the unpolarized N $2p_z$ states and via π -type overlap of the Ni2 $3d_{xz,yz}$ and the polarized N $2p_{x,y}$ orbitals. Finally, we observe overlap of like-spin $3d_{xz,yz}$ orbitals of both Ni sites. While the Ni1 $3d_{xz,yz}$ orbitals do not carry any magnetic moment they could nevertheless give rise to ferromagnetic superexchange interaction of neighboring Ni2 sites both within the Ni2 planes and across. Taken together, the just mentioned different kinds of exchange interactions establish long-range three-dimensional magnetic order. Note that this complex magnetic behavior is a mere consequence of the insertion of nitrogen since face-centered tetragonal elemental Ni would show strong ferromagnetism as pointed out above. Finally, since the interplay of the out-of-plane σ -type and π -type exchange interactions may be rather sensitive to the value of the tetragonal c axis, thin films are likely to show different magnetic properties than bulk samples as was indeed observed. In addition, this sensitivity may be responsible for the observed spin-glass like behavior. Of course, it would be exciting to have our results corroborated by new experimental data.

C. NiN

As for the other two compounds, in a first step the structural stability of NiN was probed by performing spin-degenerate GGA structure relaxations. Motivated by conflicting theoretical and experimental results regarding the relative stability of the zincblende and rock-

salt structures of the transition-metal nitrides,^{2,32,65–67} we took different crystal structures into account, namely, the rocksalt (RS), zincblende (ZB), cesium chloride (CC), and wurtzite (WZ) structure. In the rocksalt and cesium chloride structures both atoms are octahedrally coordinated by the respective other species, whereas in the zincblende and wurtzite structures the coordination by the respective other species is tetrahedral. The results of the structure relaxations are summarized in Tab. I. Again, the enthalpies of formation are calculated with

TABLE I: Structural parameters and enthalpies of formation as resulting from GGA calculations for NiN in the rocksalt (RS), cesium chloride (CC), zincblende (ZB), and wurtzite (WZ) structures.

	RS	ZB	CC	WZ
$a/\text{\AA}$	4.063	4.321	2.542	3.017
$c/\text{\AA}$				5.129
u				0.3745
E_{coh}/eV	+1.25	+0.86	+2.20	+0.90

respect to the total energies of the elements in their standard states. Note the trend of the enthalpies of formation to increase on going from Ni₃N to Ni₂N and finally to NiN, which nicely explains the observed higher thermodynamic stability of Ni₃N as compared to the N-rich nitrides. In particular, from the GGA calculations for NiN all structures listed in Tab. I are found thermodynamically highly unstable. Nevertheless, according to Tab. I, NiN has the lowest total energy in the zincblende structure in agreement with previous calculations.^{32,33} In contrast, the wurtzite structure is found at a slightly elevated energy, whereas the other two structures are much higher in energy. Unfortunately, no experimental structure determination is available, which our results could be compared to. However, since the neighboring transition-metal nitrides are found in the rocksalt structure, the above finding of the zincblende structure as the most stable one leaves some doubt. In passing, we mention that additional spin-polarized ferromagnetic calculations led to vanishing magnetic moments for all structures.

Calculated electronic densities of states as obtained from the ASW method for the rocksalt and zincblende structure, respectively, are displayed in Figs. 6 and 7. In the rocksalt structure, octahedral arrangement of the Ni atoms by nitrogen causes strong σ -type overlap of the Ni $3d e_g$ states with the N $2p$ orbitals, which leads to bonding and antibonding manifolds between about -8.5 eV and -3 eV and above -0.5 eV, respectively, while the rather non-bonding Ni $3d t_{2g}$ states form sharp peaks in between. The situation is quite similar in the zincblende structure except for the exchanged roles of the e_g and t_{2g} orbitals due to the tetrahedral rather than octahedral arrangement. For the same reason, the partial densities of states obtained for the cesium chloride and wurtzite structure are quite similar to those of the rocksalt and zincblende structure, respectively.

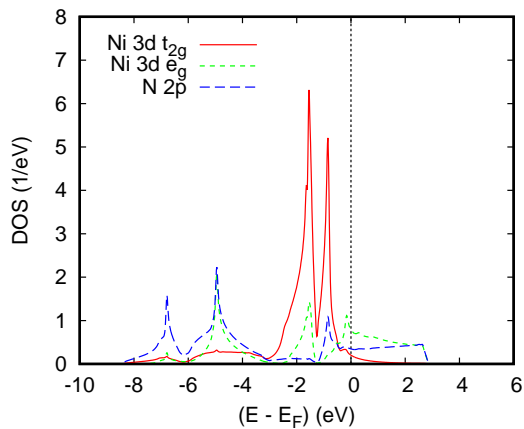


FIG. 6: Partial densities of states of NiN in the rocksalt structure as arising from the GGA calculations.

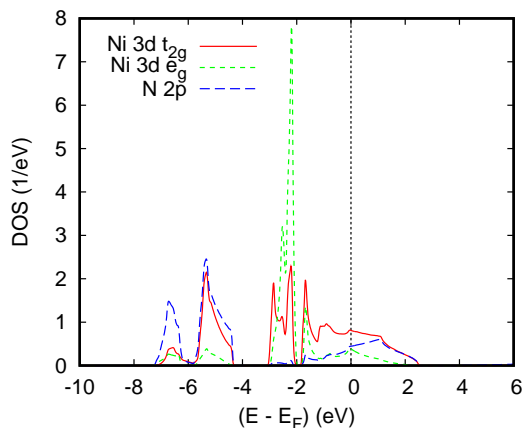


FIG. 7: Partial densities of states of NiN in the zincblende structure as arising from the GGA calculations.

Motivated by the controversial discussion regarding the ground state structure and the importance of taking into account local electronic correlations for a correct description of the electronic and magnetic properties of NiO, we complemented as before the above calculations by GGA+ U calculations for NiN. Again, all candidate structures were initially relaxed with the results summarized in Tab. II. Obviously, the changes on including local electronic correlations are threefold. While the zincblende, cesium chloride, and wurtzite structure experience a volume decrease due to the stronger localization of the Ni 3d states, the rocksalt structure shows a volume increase. The latter is related to the emergence of long-range ferromagnetic order arising from the local moments at the Ni sites. At the same time, the magnetic order induces a stabilization of the rocksalt structure, which becomes lowest in energy. However, despite this considerable downshift, even within the GGA+ U approach the enthalpies of formation are still all positive, which explains the fact that

TABLE II: Structural parameters, enthalpies of formation, and local magnetic moment at the Ni site as resulting from GGA+ U calculations for NiN in the rocksalt (RS), cesium chloride (CC), zincblende (ZB), and wurtzite (WZ) structures.

	RS	ZB	CC	WZ
$a/\text{\AA}$	4.115	4.241	2.496	2.957
$c/\text{\AA}$				5.049
u				0.3742
E_{coh}/eV	+0.52	+0.99	+2.22	+1.03
m_{Ni}/μ_B	1.3	0.0	0.0	0.0

the late 3d transition-metal nitrides have not yet been investigated experimentally. Yet, as already mentioned for Ni₂N, preparation of samples with reduced dimensionality or of nanostructures may still be possible.

These results perfectly complement those obtained for MnN, where GGA/LDA calculations led to a spin-degenerate zincblende structure as the ground state,^{65,66} in contradiction with the antiferromagnetic distorted rocksalt structure observed experimentally,⁶⁸ and the discrepancy had been resolved by GGA+ U calculations, which reproduced the experimental findings.⁶⁷

The electronic densities of states as arising from spin-degenerate GGA+ U calculations for the so relaxed rocksalt and zincblende structures closely resemble those shown in Figs. 6 and 7 except for an overall downshift of the π -type non-bonding states by about 1 eV relative to the bonding and antibonding states resulting from the σ -type overlap of the Ni 3d and N 2p states. The same holds true for the densities of states obtained from GGA+ U calculations for the cesium chloride and wurtzite structures.

The partial densities of states found from spin-polarized ferromagnetic calculations for the rocksalt structure are displayed in Fig. 8. There, we recognize

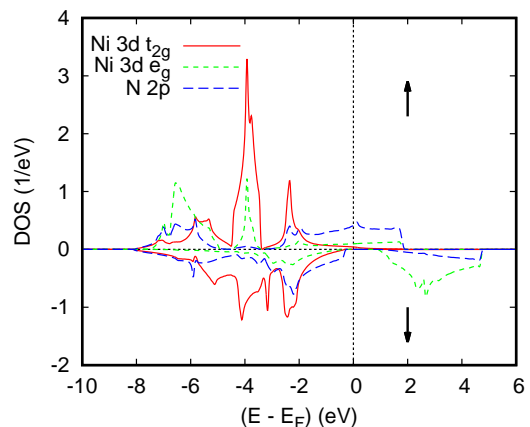


FIG. 8: Partial densities of states of NiN in the rocksalt structure as arising from the GGA+ U calculations.

for both spin channels the sequence of bonding and anti-

bonding Ni $3d e_g$ and N $2p$ states embracing the weakly π -bonding Ni $3d t_{2g}$ levels as already observed in Fig. 6. As a consequence, the latter states are fully occupied and the local magnetic moment of $1.3\mu_B$ is carried exclusively by the e_g states. The imbalance between the spin-up and spin-down e_g electrons is connected with the fact that in the spin-majority channel the σ -type bonding and antibonding states are dominated by the Ni $3d e_g$ and N $2p$ states, respectively, whereas in the spin-minority channel this is reversed. As a consequence, the nitrogen sites carry a small magnetic moment of $-0.3\mu_B$, which leads to a total magnetic moment per formula unit of $1.0\mu_B$. Finally, crystal-field splitting causes opening of a band gap of almost 1.2 eV in the spin-minority spectrum, which leaves NiN as a half-metallic ferromagnet much like, e.g. CrO₂, which belongs to the most-investigated materials of this exciting class.⁶⁹⁻⁷¹

As expected, results obtained from additional GGA+ U calculations with $U = 4.0$ eV and $J = 0.64$ eV are found between those arising from the GGA and the above described GGA+ U calculations. In particular, the volume increase on going from GGA to GGA+ U as mentioned above is reduced as is the stability of the rocksalt structure as compared to the zincblende structure. At the same time, the gap in the spin-minority channel is also reduced and shifted slightly below the Fermi energy while the local magnetic moments carried by Ni and N are reduced to about $1.1\mu_B$ and $-0.1\mu_B$, respectively. As a deeper analysis revealed, these changes result to a large part from the shrinking of the lattice coming with the reduction of the local-correlation parameters. In contrast, variation of U and J while keeping the lattice parameter at the value given in Tab. II preserves the half-metallic behavior to much lower values of these parameters. Nevertheless, in closing we point out that for $U = 6.0$ eV and $J = 0.95$ eV as determined and adopted by most researchers the calculations clearly show the half-metallic behavior described above.

Finally, we mention spin-polarized GGA and GGA+ U calculations starting from antiferromagnetic order with a spin-propagation vector along either the $\langle 001 \rangle$ or the $\langle 111 \rangle$ direction for the cubic structures and along the $\langle 0001 \rangle$ direction in case of the wurtzite structure, neither of which converged to a stable antiferromagnetic state. In addition, we were not able to stabilize antiferromagnetic order in the tetragonally distorted rocksalt and zincblende structures, contrary to the antiferromagnetic alignment found for CrN and MnN, respectively,

with orthorhombically and tetragonally distorted rocksalt structure.^{34,67}

IV. CONCLUSION

The nickel nitrides Ni₃N, Ni₂N, and NiN have been investigated by means of first principles electronic structure calculations as based on density functional theory. Both the generalized gradient approximation (GGA) and the GGA+ U approach were used. While for Ni₃N the results obtained from both schemes are very similar, taking into account local electronic correlations via the GGA+ U approach turned out critical especially for the correct description of the magnetic properties of the N-rich compounds.

For NiN, a structural phase study including the rocksalt, zincblende, cesium chloride, and wurtzite structures led to diverse results. Whereas from GGA calculations the zincblende structure was found most stable with a non-magnetic metallic ground state, GGA+ U calculations led to a half-metallic ferromagnet crystallizing in the rocksalt structure as the lowest-energy state. This result is in line with both experimental and theoretical findings for the neighboring transition-metal nitrides and calls for experimental confirmation, in particular in view of possible exciting applications of this material in spin-filtering devices.

For Ni₂N, which crystallizes in a simple tetragonal lattice, GGA calculations again found a non-magnetic metallic state contrasting experimental observations, whereas from GGA+ U calculations ferrimagnetic order with antiparallel alignment of the moments at the two Ni sites and substantial polarization of the N p states was obtained. Coupling of the Ni magnetic moments is via complex interplay of three-dimensional exchange interactions, which fact may explain the reported sensitivity of the magnetic order to details of the crystal structure. Again, refined experiments are called for to confirm our predictions.

Acknowledgments

A.H. gratefully acknowledges financial support of Bejaia University.

* corresponding author: abdeslam.houari@univ-bejaia.dz

† s.matar@lgu.edu.lb

‡ veyert@materialsdesign.com

¹ L. E. Toth, *Transition Metal Carbides and Nitrides*, (Academic Press, New York 1971).

² H. Shimizu, M. Shirai, and N. Suzuki, J. Phys. Soc. Japan **66**, 3147 (1997).

³ N. S. Gajbhiye, R. S. Ningthoujam, and J. Weissmüller, phys. stat. sol. (a) **189**, 691 (2002).

⁴ A. Fernández Guillermet and K. Frisk, J. Alloys Compounds **203**, 77 (1994).

⁵ A. Fernández Guillermet and K. Frisk, Inter. J. Thermophys. **12**, 417 (1991).

⁶ I. M. Neklyudov and A. N. Morozov, Physica B **350**, 325

- (2004).
- 7 R. Juza and W. Sachsze, *Z. Anorg. Allg. Chem* **251**, 201 (1943).
 - 8 A. Leineweber, H. Jacobs, W. Kockelmann, and S. Hull, *Physica B* **276**, 266 (2000).
 - 9 A. Leineweber, H. Jacobs, and S. Hull, *Inorg. Chem.* **40**, 5818 (2001).
 - 10 A. Leineweber, H. Jacobs, W. Kockelmann, S. Hull, and D. Hinz-Hübner, *J. Alloys Compounds* **384**, 1 (2004).
 - 11 G. Dorman and M. Sikkens, *Thin Solid Films* **105**, 251 (1983).
 - 12 D. Vempaire, S. Miraglia, A. Sulpice, L. Ortega and E. K. Hill, D. Fruchart, and J. Pelletier, *J. Magn. Magn. Mat.* **272-276**, e843 (2004).
 - 13 C. Guillaume, J. P. Morniroli, D. J. Frost, and G. Serghiu, *J. Phys.: Condens. Matter* **18**, 8651 (2006).
 - 14 D. Vempaire, S. Miraglia, J. Pelletier, D. Fruchart, E. K. Hill, L. Ortega, A. Sulpice, and F. Fettar, *J. Alloys Compounds* **480**, 225 (2009).
 - 15 D. Vempaire, F. Fettar, L. Ortega, F. Pierre S. Miraglia, A. Sulpice, J. Pelletier, E. K. Hill, and D. Fruchart, *J. Appl. Phys.* **106**, 073911 (2009).
 - 16 E. Lindahl, M. Ottosson, and J.-O. Carlsson, *ECS Trans.* **25**, 365 (2009).
 - 17 N. Popovic, Z. Bogdanov, B. Goncic, S. Strbac, and Z. Rakocevic, *App. Surf. Science* **255**, 4027 (2009).
 - 18 A. Leineweber, F. Liebert, S. L. Shang, Z.-K. Liu, and E. J. Mittemeijer, *J. Mater. Res.* **27**, 1531 (2012).
 - 19 L. Maya, *J. Vac. Sci. Techn.* **11**, 604 (1993).
 - 20 C. M. Fang, M. H. F. Sluiter, M. A. van Huis, and H. W. Zandbergen, *Phys. Rev. B* **86**, 134114 (2012).
 - 21 Y. Imai, M. Sohma, and T. Suemasu, *J. Alloys Compounds* **611**, 440 (2014).
 - 22 P. N. Terao, *J. Phys. Soc. Japan* **15**, 227 (1960).
 - 23 S. Nagakura, N. Otsuka, and Y. Hirotsu, *J. Phys. Soc. Japan* **35**, 1492 (1973).
 - 24 Y. Kong and F. Li, *Phys Rev. B* **57**, 970 (1998).
 - 25 P. Hemzalova, M. Friak, M. Sob, D. Ma, A. Udyansky, D. Raabe, and J. Neugebauer, *Phys. Rev. B* **88**, 174103 (2013).
 - 26 M. Meinert, *J. Phys. Condens. Matter* **28**, 056006 (2016).
 - 27 S. Matar, P. Mohn, G. Demazeau, and B. Siberchicot, *J. Phys. France* **49**, 1761 (1988)
 - 28 P. Mohn, K. Schwarz, S. Matar, and G. Demazeau, *Phys. Rev. B* **45**, 4000 (1992).
 - 29 A. Houari, S. F. Matar, and M. A. Belkhir, *J. Magn. Magn. Mat.* **312**, 298 (2007).
 - 30 P. Monachesi, T. Björkman, T. Gasche, and O. Eriksson, *Phys. Rev. B* **88**, 054420 (2013).
 - 31 H. Nishihara, K. Suzuki, R. Umetsu, T. Kanomata, T. Kaneko, M. Zhou, M. Tsujikawa, M. Shirai, T. Sakon, T. Wada, K. Terashima, and S. Imada, *Physica B* **449**, 85 (2014).
 - 32 H. Wang and D. S. Xue, *Chin. Phys. Lett.* **21**, 1612 (2004).
 - 33 C. Paduani, *Solid State Commun.* **148**, 297 (2008).
 - 34 A. Mavromaras, S. Matar, B. Siberchicot, and G. Demazeau, *J. Magn. Magn. Mater.* **134**, 34 (1994).
 - 35 S. F. Matar, A. Houari, and M. A. Belkhir, *Phys. Rev. B* **75**, 245109 (2007).
 - 36 A. Houari, S. F. Matar, M. A. Belkhir, and M. Nakhil, *Phys. Rev. B* **75**, 064420 (2007).
 - 37 A. Houari, S. F. Matar, and M. A. Belkhir, *Comp. Mat. Sci.* **43**, 392 (2008).
 - 38 A. Houari, S. F. Matar, and V. Eyert, *Phys. Rev. B* **82**, 241201 (2010).
 - 39 A. Houari, S. F. Matar, and M. A. Belkhir, *J. Magn. Magn. Mat.* **322**, 658 (2010).
 - 40 P. Hohenberg and W. Kohn, *Phys. Rev.* **136**, B864 (1964).
 - 41 W. Kohn and L. J. Sham, *Phys. Rev.* **140**, A1133 (1965).
 - 42 J. P. Perdew, K. Burke, and M. Ernzerhof, *Phys. Rev. Lett.* **77**, 3865 (1996); *Phys. Rev. Lett.* **78**, 1396(E) (1997).
 - 43 V. I. Anisimov, J. Zaanen, and O. K. Andersen, *Phys. Rev. B* **44**, 943 (1991).
 - 44 A. I. Liechtenstein, V. I. Anisimov, and J. Zaanen, *Phys. Rev. B* **52**, R5467 (1995).
 - 45 F. Zhou, M. Cococcioni, C. A. Marianetti, D. Morgan, and G. Ceder, *Phys. Rev. B* **70**, 235121 (2004).
 - 46 A. Jain, G. Hautier, S. P. Ong, C. J. Moore, C. C. Fischer, K. A. Persson, and G. Ceder, *Phys. Rev. B* **84**, 045115 (2011).
 - 47 P. Seth, P. Hansmann, A. van Roekeghem, L. Vaugier, and S. Biermann, *Phys. Rev. Lett.* **119**, 056401 (2017).
 - 48 S. Ryee and M. J. Han, *Sci. Rep.* **8**, 9559 (2018).
 - 49 V. I. Anisimov, I. V. Solovyev, M. A. Korotin, M. T. Czyżyk, and G. A. Sawatzky, *Phys. Rev. B* **48**, 16929 (1993).
 - 50 M. T. Czyżyk and G. A. Sawatzky, *Phys. Rev. B* **49**, 14211 (1994).
 - 51 I. V. Solovyev, P. H. Dederichs, and V. I. Anisimov, *Phys. Rev. B* **50**, 16861 (1994).
 - 52 G. Kresse and J. Furthmüller, *Phys. Rev. B* **54**, 11169 (1996); *Comput. Mater. Sci.* **6**, 15 (1996).
 - 53 MedeA[®] 2.22, Materials Design, Inc. (2018).
 - 54 P. E. Blöchl, *Phys. Rev. B* **50**, 17953 (1994).
 - 55 G. Kresse and D. Joubert, *Phys. Rev. B* **59**, 1758 (1999).
 - 56 H. J. Monkhorst and J. D. Pack, *Phys. Rev. B* **13**, 5188 (1976).
 - 57 V. Eyert, *Int. J. Quantum Chem.* **77**, 1007 (2000).
 - 58 V. Eyert, *The Augmented Spherical Wave Method*, Lect. Notes Phys. **849** (Springer, Berlin Heidelberg 2013).
 - 59 V. Eyert and K.-H. Höck, *Phys. Rev. B* **57**, 12727 (1998).
 - 60 V. Eyert, *J. Comput. Phys.* **124**, 271 (1996).
 - 61 P. E. Blöchl, O. Jepsen, and O. K. Andersen, *Phys. Rev. B* **49**, 16223 (1994).
 - 62 Z. Ma, H. Zhang, X. Sun, J. Guo, and Z. Li, *Appl. Surf. Science* **420**, 196 (2017).
 - 63 N. W. Ashcroft and N. D. Mermin, *Solid State Physics* (Holt-Saunders, Philadelphia 1976)
 - 64 A. I. Linnik, A. M. Prudnikov, R. V. Shalaev, T. A. Linnik, V. N. Varyukhin, S. A. Kostyrya, and V. V. Burkhovetskii, *Techn. Phys. Lett.* **39**, 143 (2013).
 - 65 H. M. Hong, Y. J. Kang, J. Kang, E. C. Lee, Y. H. Kim, and K. J. Chang, *Phys. Rev. B* **72**, 144408 (2005).
 - 66 M. S. Miao and W. R. L. Lambrecht, *Phys. Rev. B* **76**, 195209 (2007)
 - 67 J. A. Chan, J. Z. Liu, H. Raebiger, S. Lany, and A. Zunger, *Phys. Rev. B* **78**, 184109 (2008).
 - 68 K. Suzuki, T. Kaneko, H. Yoshida, Y. Obi, H. Fujimori, and H. Morita, *J. Alloys Compounds* **306**, 66 (2000).
 - 69 S. Matar, G. Demazeau, J. Sticht, V. Eyert, and J. Kübler, *J. Phys. I France* **2**, 315 (1992); *J. Phys. I France* **4**, 1259 (1994).
 - 70 S. Matar, V. Eyert, J. Sticht, J. Kübler, and G. Demazeau, *J. Phys. I France.* **4**, 1199 (1994).
 - 71 F. Bisti, V. A. Rogalev, M. Karolak, S. Paul, A. Gupta, T. Schmitt, G. Güntherodt, V. Eyert, G. Sangiovanni, G. Profeta, and V. N. Strocov, *Phys. Rev. X* **7**, 041067 (2017).